Passive Shear Layer Regularization Experiments in Wind Tunnels and Feed-Forward Adaptive-Optic Correction

Donald J. Wittich, III [1], Daniel A. Duffin[5]
and Eric J. Jumper[2]
University of Notre Dame, Notre Dame, Indiana, 46556

Alan B. Cain [3]
Innovative Technology Applications Company, LLC, Chesterfield, Missouri, 63006

Edward J. Kerschen [4]
University of Arizona, Tucson, Arizona, 85721

Shear layer regularization is a fundamental requirement in a Feed-Forward, Adaptive-Optic (FFAO) wavefront correction scheme applied to a beam passing through the shear layer. 'Passive regularization' exploits the self-sustained oscillations of a shear layer over a resonant cavity, thereby eliminating the need for active flow control actuation. In wind tunnel tests, a strong acoustic resonance coupled with the cavity shear layer feedback mechanism produced a robust, predictable shear layer motion. The unsteady pressure at the upstream wall of the cavity was periodic enough to be used as a reliable phase reference. This phase reference was used to drive a phase-locked wavefront acquisition system and, ultimately, a deformable mirror which applied a feed-forward wavefront correction. The source of the strong acoustic resonance resulted from trapped duct modes, a result of the particular cavity and wind tunnel geometry combination. Unsteady pressure data indicated that this otherwise undesirable source of resonance can be mitigated by lining the wind tunnel wall opposite the cavity with an acoustically absorbent material.

Nomenclature

α	empirical constant
a_0	stagnation speed-of-sound
D	cavity depth
DM	deformable mirror
f	frequency
FFAO	feed-forward, adaptive-optic
$f_{CT\,cr}$	critical cut-on frequency for the cavity-tunnel region
$f_{T\,cr}$	critical cut-on frequency for the tunnel region
k	empirical constant, convective speed ratio (U_c/U_∞)
L	cavity streamwise length
m	integer mode number
M_∞	freestream Mach number
OPD	optical path difference
PSD	position sensing device or power spectral density
U_c	shear layer convective velocity
U_∞	freestream velocity
I	on-axis, far-field beam intensity
I_0	on-axis, far-field, diffraction-limited beam intensity

[1] PhD Candidate, Aerospace and Mechanical Engineering, 118 Hessert Laboratory, AIAA Student Member.
[2] Professor of Aerospace and Mechanical Engineering, 124 Hessert Laboratory, AIAA Member.
[3] President, P.O. Box 6971, AIAA Member.
[4] Professor of Aerospace and Mechanical Engineering, PO Box 210119, AIAA Member.
[5] PhD Candidate, Aerospace and Mechanical Engineering , B018 Hessert Laboratory.

I. Introduction

The shear layer that forms when air flow separates from a surface at high subsonic Mach number contains a rapidly varying index-of-refraction (i.e. density) field. When this field is near the exit aperture of a light source such as a laser, the effects of the field are referred to as 'aero-optic' effects[1]. Aero-optic effects include the highly unsteady wavefront deformations imparted by the aero-optic field and their resulting far-field patterns. In this paper, the wavefront deformation is described by its optical path difference *OPD*, which has units of length, and the far-field performance is described by the Strehl ratio which relates the beam's on-axis intensity, *I*, to the diffraction limited intensity, I_0, which would result if there was no wavefront distortion. The rapidly varying nature of the shear layer has thus far prevented attempts to mitigate the aero-optic effects with traditional adaptive-optics[2]. Feed-Forward Adaptive-Optic (FFAO) wavefront correction has been demonstrated as an alternative mitigation scheme[3]. FFAO does not suffer the bandwidth limitations of traditional adaptive-optic systems but requires *a priori* knowledge of the aero-optic deformation. Shear layer 'regularization' means that the shear layer is forced into a predictable, repeating pattern for which phase and amplitude are the remaining unknowns. Active shear layer regularization involves relatively high frequency actuation of sufficient amplitude near the point of separation[4]. Passive regularization, in this context, exploits the self-sustained oscillations of a shear layer over a resonant cavity.

Cavity Oscillations: The strong, unsteady pressure fluctuations associated with subsonic and supersonic flow over a cavity have long been an undesirable feature of aircraft with exposed, internal weapons bays. This study involved a shallow (L/D = 4) cavity in compressible subsonic flow, similar to those studied by Krishnamurty[5], Roshko[6], Plumblee *et al.*[7], Rossiter[8], Heller *et al.*[9] among numerous others. Rossiter proposed a model of vortex-type structures in the shear layer propagating downstream at a speed U_c with $k = U_c/U_\infty$. These structures impinge on the downstream edge of the cavity, generating acoustic disturbances which propagate back upstream to further promote periodic oscillations in the shear layer. Using this simple model, Rossiter developed the semi-empirical formula

$$\frac{fL}{U_\infty} = \frac{m-\alpha}{M_\infty + 1/k}, \quad (m = 1, 2, 3, \text{etc.}) \tag{1}$$

which relates the Strouhal number (frequency, *f*, cavity length, *L*, and freestream velocity, U_∞) to an integer mode number *m*, the freestream Mach number M_∞, the convective speed ratio *k* and a phase relationship α. The values for α and *k*, are often chosen best fit the data. The non-harmonic, integer modes associated with *m* are often referred to as Rossiter modes. Heller *et al.*[9] modified Rossiter's formula (Equation 1) to extend it to a higher range of Mach number with a temperature correction to the Mach number. The resulting equation,

$$\frac{fL}{U_\infty} = \frac{m-\alpha}{M_\infty\left(1+[(\gamma-1)/2]M_\infty^2\right)^{-1/2} + 1/k} \quad (m = 1, 2, 3, \text{etc.}) \tag{2}$$

is sometimes called the modified Rossiter equation. Equation 2, with α = 0.25 was used throughout this work as a frequency prediction tool. Although a Malley Probe has the capability to measure *k* at a single, streamwise location within the cavity, *k* was generally chosen to fit the unsteady pressure data.

The feedback type forcing described by the Rossiter equation can be altered and amplified by acoustic resonances within or near the cavity[10]. Acoustic energy generated by the cavity oscillations and directed outward from the cavity would radiate away in an open environment whereas a solid wall opposite the cavity inhibits radiation. Therefore, the acoustic energy generated in the cavity must escape the cavity-tunnel region through the inlet and exit ducts. For a "cavity-in-wall" geometry like the one used here, a problem arises when the excited acoustic frequency is above the critical, cut-on frequency of the larger cavity-tunnel region, $f_{CT_{cr}}$, but below the critical, cut-on frequency of the smaller tunnel region, $f_{T_{cr}}$. The acoustic field becomes "trapped" in the cavity-tunnel region, resulting in very high amplitudes[11]. More detailed descriptions of trapped modes and theoretical analyses are available in Alvarez and Kerschen[12] and Kerschen and Cain[11]. The latter reference shows that trapped modes are more prevalent in cavity-tunnel geometries where the cavity is depth is significant compared to the height of the inlet and exits.

II. Experimental Setup

The wind tunnel experiments described here were performed in two phases at the Hessert Laboratory at the University of Notre Dame. The Phase 1 experiments included pressure and optical measurements, and culminated with a demonstration of FFAO wavefront correction. The Phase 2 experiments included more unsteady pressure measurements to examine the effect of trapped duct modes on the Phase 1 experiments. Both phases were conducted using an in-draft wind tunnel similar to the configuration shown in Figure 1. Air is drawn through a 150:1 contraction inlet into a rectangular test section measuring 9.9 x 10 cm. The flow then passes through diffuser section to vacuum pumps housed in a separate room.

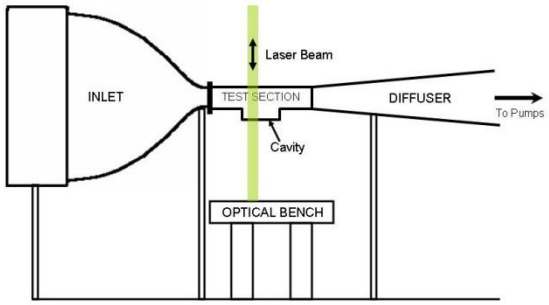

Figure 1: General wind-tunnel arrangement

The Phase 1 test section (Figure 2A) was constructed primarily of aluminum and optical glass. The cavity was formed by a displaced section of the cavity wall with a depth, D of 3.81 cm and length, L of 15.24 cm (L/D = 4). Kerschen and Cain[11] refer to this as a "cavity-in-wall geometry". The ratio of the cavity depth to the tunnel height was 0.375, the largest ratio considered in the theoretical analysis of Ref. 11. The floor, roof and side-walls of the cavity were constructed from 1.9 cm thick optical glass. Seven static pressure ports were mounted upstream and along the length of the cavity to measure the incoming and external (to the cavity) flow static pressures with a Mercury-based, U-tube manometer. Unsteady pressure tranducers (Kulites) were mounted in both the forward and aft walls of the cavity to provide fluctuating pressure data within the cavity. A Vishay 2310 signal conditioner provided each Kulite with a Wheatstone bridge circuit, excitation voltage, gain control, AC coupling and voltage output. The voltage output from the signal conditioner was acquired with a PC-based, Microstar data acquisition system at a 100 kHz sampling frequency.

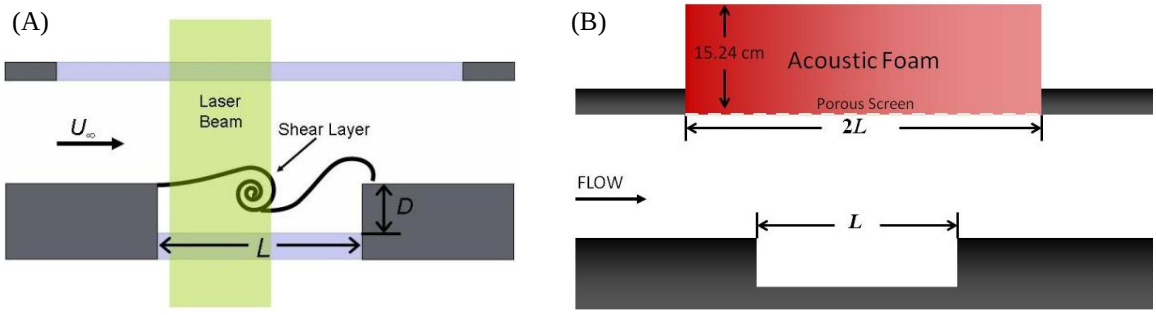

Figure 2: Illustrations of Phase 1 (A) and Phase 2 (B) test sections. The lightly shaded walls of the Phase 1 test section represent the optical windows. The acoustic "muffler" on the upper wall of the Phase 2 test section could be replaced with a solid Plexiglas wall, restoring a geometry nearly identical to that of Phase 1.

The Phase 2 test section included another cavity-in-wall geometry constructed almost entirely from Plexiglas. The cavity was 15.24 cm long and 3.71 cm deep, slightly shallower than the Phase 1 cavity. In addition, the Plexiglas along the upper wall of the test section (opposite the cavity) could be replaced with a porous steel screen backed by 15.24 cm of open cell, acoustic damping foam, shown in Figure 2B. This acoustically treated wall extended $L/2$ upstream and downstream of the cavity ends. Kulite unsteady pressure sensors were mounted in seven

different locations, including the centers of the upstream and downstream cavity walls. Static wall pressures were measured by differential pressure transducers at four streamwise locations, one near the inlet and three more spaced at approximately 7.6 cm ($L/2$) over the upstream lip, middle and downstream lip of the cavity. Because the cavity causes some blockage in the tunnel, the flow accelerates over the length of the cavity. The "freestream" static pressure was therefore taken to be the average of the three values acquired over the length of the cavity opening. All of the pressure data (unsteady and static) were acquired simultaneously by a PC-based Microstar data acquisition system with a sampling rate of 50 kHz for 5×10^5 samples.

Aero-Optic Measurements: Aero-optic data were acquired only during Phase 1. The aero-optic wavefront disturbances were measured with two devices, a Malley Probe, originally described by Gordeyev *et al.*[13], and a Wavefront Sciences CLAS-2D Shack-Hartmann wavefront sensor. The Malley Probe utilized two small diameter (~1mm) beams, propagated normal to the shear layer and spaced closely together in the flow direction. Because the beams are of such small diameter, all relevant aero-optic disturbances are manifested as beam jitter. By correlating the two beam jitter signals, the convective velocity, U_c, of the aberrating structure can be computed. The jitter time series acquired from each beam can be used to extract temporal frequency information. The beams were propagated from the optical table, through the flow and then reflected back along their incoming path. This double path through the shear layer increased the signal-to-noise ratio. The beams were then focused onto photo-detectors called Position Sensing Devices (PSD's) where the jitter was measured as spot displacement. Photons incident on each PSD generated currents which were fed to a trans-impedance amplifier where the signals were converted to voltages and low-pass filtered at 50 kHz to avoid frequency aliasing. The output voltages were acquired at 100 kHz by the same Microstar system described above.

Instantaneous, two-dimensional wavefronts of the shear layer were acquired using a Wavefront Sciences CLAS-2D, Shack-Hartmann wavefront sensor with a 44 x 33 lenslet array. The sensor was illuminated by a frequency doubled Nd:YAG pulsed laser with an approximately 6 ns pulse duration. Although the CLAS-2D system is incapable of producing temporally resolved wavefronts of the aberration cycle, it was possible to trigger the system to capture wavefronts at a constant phase of the unsteady pressure disturbance cycle. In this case, the system was triggered by the upstream Kulite or Malley Probe signal, as described in the next section. The strong periodicity of the signal allowed acquisition of wavefronts at 12 phase angles, in 30° increments, covering one complete cycle of the shear layer oscillation. Two-hundred individual wavefronts were acquired at each phase angle. A Fourier optics code was then employed to convert the wavefront measurements into realizations of the far-field intensity distributions.

Adaptive Optics System: The core adaptive-optics system used in this work was the same as that described in References 3, 14 and 15. The centerpiece of the system is a 49 mm diameter, 37 actuator, Xinetics deformable mirror (DM). The piezoelectric actuators have a stroke of +/- 4 μm and can be driven linearly to frequencies above 5 kHz. In comparison, the relevant aero-optic disturbances possessed *OPD* values in the range of +/- 0.4 μm, with disturbance cycle frequencies under 1200 Hz. For this work, the DM was de-coupled from its traditional adaptive-optics system and driven with pre-programmed inputs from a thirty-seven channel digital-to-analog system, using five National Instruments NI PXI-6733, 8-channel, 16-bit, analog-output boards. These signal generators were driven with digital time histories obtained from the post-processed, phase-locked, averaged *OPD* results, producing the necessary conjugate corrections on the DM. This feed-forward system is described in much greater detail in References 3 and 14. Further details of the actuator responses can be found in Reference 15. Figure 3 shows a simplified schematic representation of the FFAO experiment optical layout which includes the laser beam train and the component relationships of the adaptive-optics system, laser, wavefront sensor and delay circuit (described below).

The primary difference between the FFAO correction scheme used in this work and those of previous FFAO experiments was the triggering scheme. Since the flow was passively forced by an aero-acoustic/hydrodynamic resonance, the disturbance phase had to be inferred from a reference pressure signal or Malley Probe jitter signal. In this case, the unsteady pressure signal from the upstream cavity wall was selected as the appropriate reference signal because of its relatively clean and strongly periodic shape. The pressure signal was band-passed filtered to isolate the primary disturbance frequency and AC coupled to prepare it for analysis. The signal was then input to a custom-built triggering delay circuit (see Figure 3) which determined the reference phase with a zero crossing analysis. Based on this reference phase, up to four programmable, independently delayed TTL pulses were output. The delays varied from 1 μs to 10^6 μs, with a 1 μs resolution. When the FFAO analog-output system received a trigger, it automatically output the data stored in the FIFO memory to the thirty-seven analog-output channels at an update rate of approximately 24 times per disturbance cycle. Ideally, a system could trigger and apply a wavefront correction at each disturbance cycle. In reality, the zero-crossings of the reference signal were not perfectly spaced according to the peak disturbance frequency. It was more practical, therefore to allow the

DM to run for ten disturbance cycles before it waited for the next trigger pulse. This helped the DM to remain locked to the flow even if the National Instruments on-board timing oscillators began to drift during the experiment.

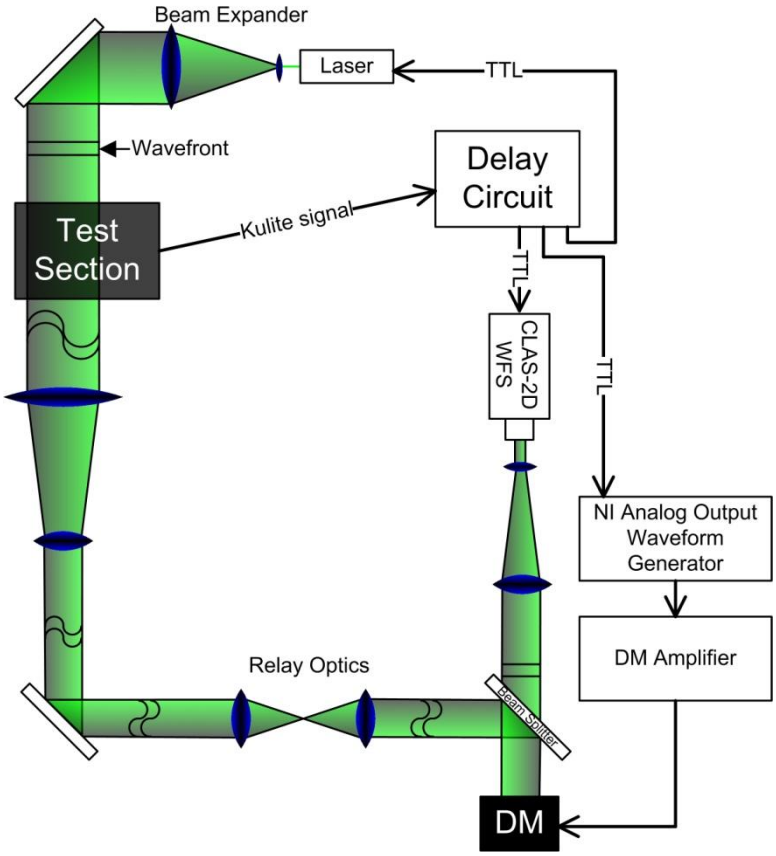

Figure 3: Optical beam train schematic for 2-D wavefront acquisition and FFAO wavefront correction.

III. Results

Phase 1 Results: The unsteady pressure (Kulite) and Malley Probe jitter spectra shown in Figure 4 indicate a dominant peak frequency near 1140 Hz at Mach 0.65 for both the pressure and optical disturbances, respectively. Both spectra also indicate a smaller peak around 430 Hz. Using the measured flow conditions, an evaluation of the Equation 2, with $\alpha = 0.25$ and $k = 0.65$ gives predicted oscillation frequencies of 492 Hz when $m = 1$ and 1147 Hz when $m = 2$. The value of $k = 0.64$ was initially chosen based on Malley Probe convection data, but $k = 0.65$ is used here because it is consistent with the value chosen in Phase 2 (below). In this case, Equation 2 seemed to accurately predict the second mode frequency, but the observed and predicted first mode frequencies differed by approximately 14%, a significant error. During Phase 2 (described later), pressure data was acquired over a range of Mach numbers, rather than at a single Mach number. The Phase 2 experiments demonstrated that the prevalence of the peak at 1140 Hz was due to a combined effect of the Rossiter-type shear layer feedback phenomenon, an acoustic resonance within the cavity and, most importantly, trapped duct modes within the cavity-tunnel region. The Phase 2 experiments also showed that Equation 2 is a poor predictor of oscillation frequencies when the wind tunnel configuration gives rise to trapped modes.

The advantage of this trapped-mode resonance was that it regularized the shear layer motion into a predictable, repeating pattern. As mentioned in the previous section, the unsteady pressure signal from the upstream cavity wall was sufficiently periodic to be used as a phase reference for the triggering delay circuit which output TTL pulses to the pulsed laser and wavefront sensor camera. This phase reference allowed for phase-locked acquisition of wavefronts and shadowgraphs. The shadowgraphs, although poor in quality, were of sufficient clarity

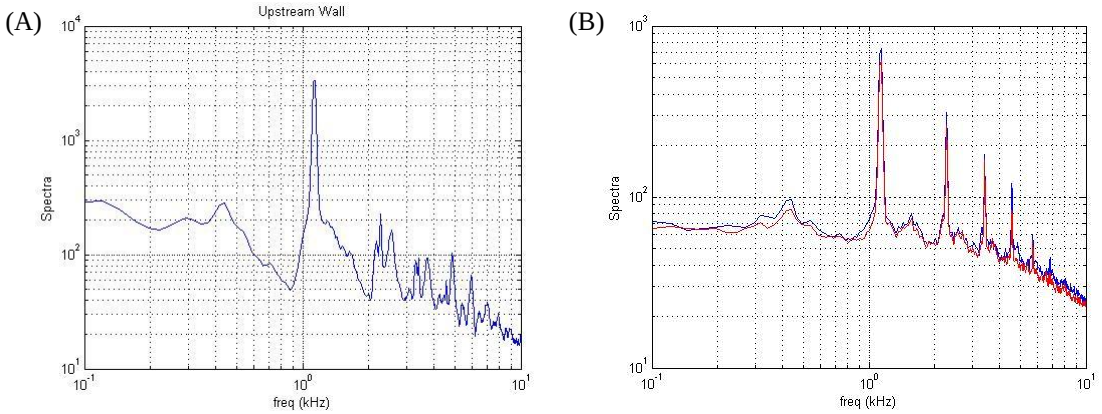

Figure 4: Amplitude spectra for unsteady pressure in the aft-facing cavity wall (A) and the Malley Probe jitter (B) for two beams passed through the center of the cavity. The two non-harmonic peaks are at ~430 Hz and 1147 Hz.

to reveal an apparently regularized flow structure. Phase-locked wavefronts were acquired at 12 phase angles over the disturbance cycle. Six phase-locked, averaged wavefronts of the uncorrected aero-optic disturbance are shown in Figure 5. These wavefronts were used to program the conjugate correction for the DM. The corrected wavefronts in Figure 6 indicate that once FFAO wavefront correction was applied, the large shear layer disturbance was removed. The overall aperture tilt of the corrected wavefronts was removed in post-processing. In a full adaptive-optic system, a tilt removal (fast-steering) mirror may be used to remove tilt after the DM correction is applied[16].

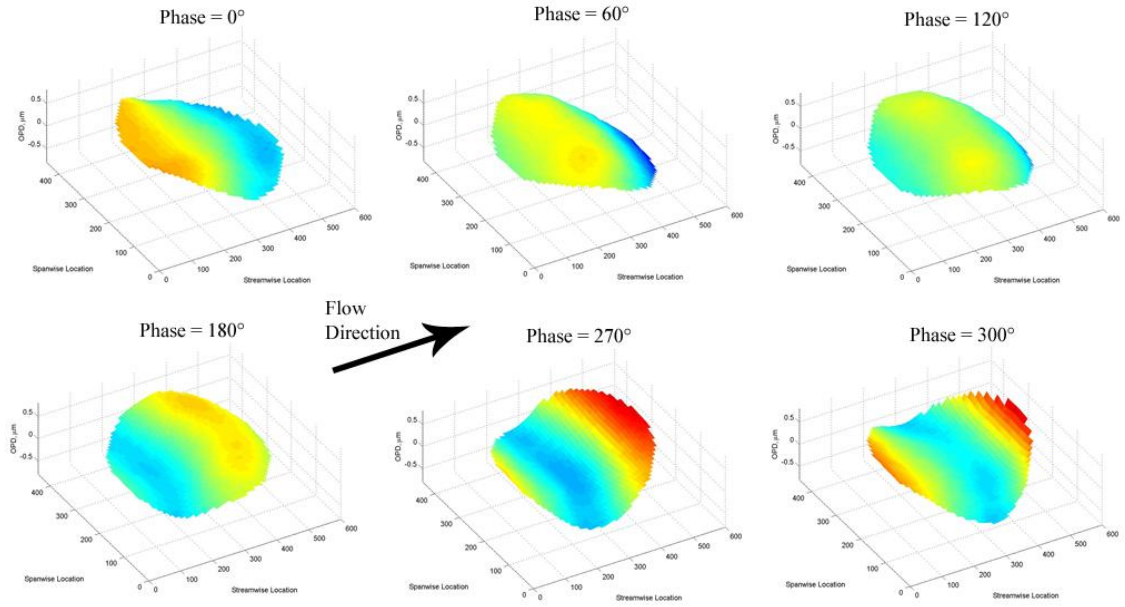

Figure 5: Phase-locked, averaged wavefronts of the uncorrected cavity shear layer.

Table 1 summarizes important wavefront statistics for both the uncorrected and FFAO corrected wavefronts. The values in Table 1 are the averages (over 12 phase angles) of the phase-locked, averaged wavefronts. Figure 7 plots the OPD_{rms} and the Strehl ratios for the phase-averaged wavefronts versus phase angle. The plots in Figure 7 indicate that the effectiveness of the FFAO correction was severely limited at the 150° and 180° phases. Figure 7B actually indicates that the FFAO correction has a negligible effect on the Strehl ratio at 150° and a negative effect at 180°. Otherwise, the FFAO correction seemed to have a significantly positive impact over the rest of the disturbance cycle. It was unclear what caused the errors evident around 180°, and they are discussed further in the *Conclusions* section.

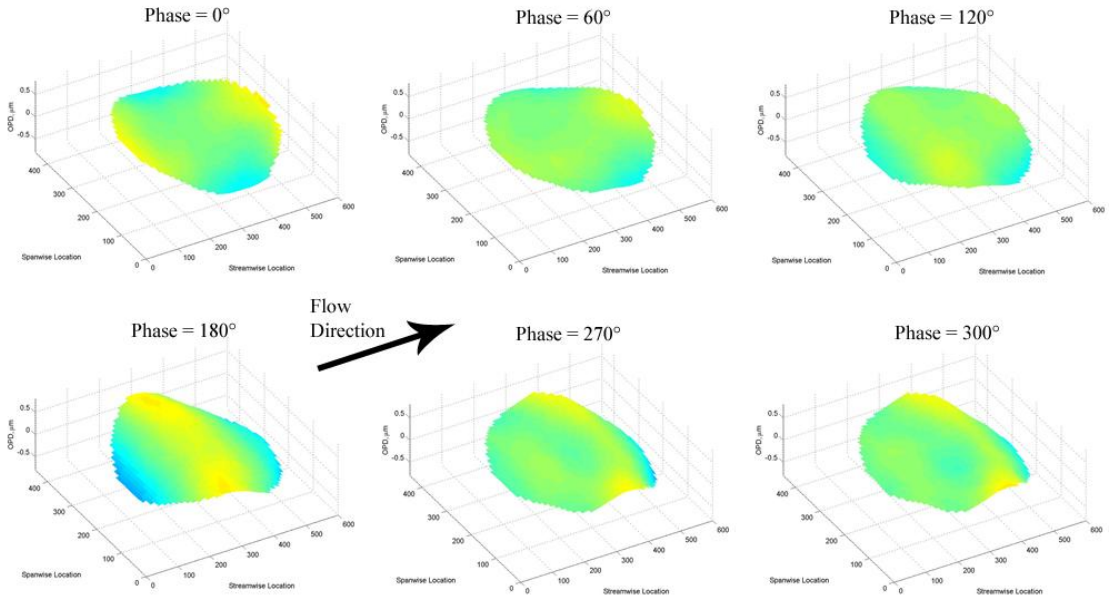

Figure 6: FFAO corrected, tilt-removed, phase-locked, averaged wavefronts of the cavity shear layer.

	Uncorrected WF	FFAO Corrected/Tilt Removed WF
OPD_{rms} (μm)	0.21	0.08
$OPD_{p\text{-}v}$ (μm)	0.77	0.46
Strehl (I/I_0)	0.28	0.75
Power-in-the-Bucket (% of diffraction limited)	51.6	80.6

Table 1: Phase-locked, averaged wavefront (WF) statistics. The values were averaged over the 12 measured phase angles.

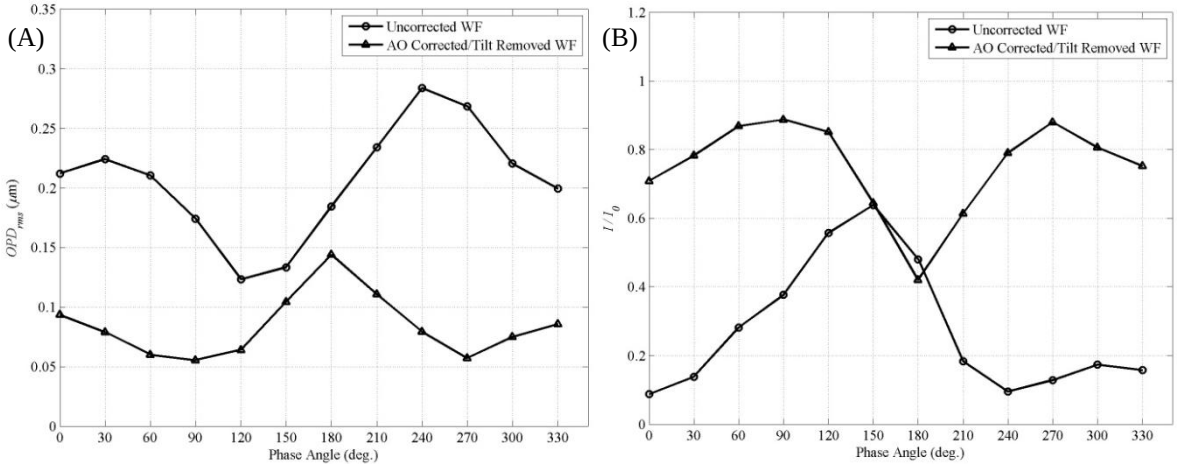

Figure 7: 2-D wavefront (WF) OPD_{rms} (A) and Strehl Ratio (B) as a function of phase angle for uncorrected and FFAO corrected/tilt-removed wavefronts.

Phase 2 Results: The unsteady pressure and wavefront results obtained during Phase 1 indicated the existence of a single, dominant peak frequency with only one other non-harmonic mode evident (and a much lower strength). This behavior of the unsteady pressure in the cavity did not appear to agree with the results of Rossiter[8] or Heller *et al*.[9] This discrepancy motivated the Phase 2 study of an almost identical geometry over a range of subsonic Mach numbers. In one experiment, the wall opposite the cavity was half-inch thick Plexiglas, and unsteady pressure data were acquired at 36 Mach numbers between 0.34 and 0.76. In a second experiment, the Plexiglas wall was replaced with the acoustic muffler shown in Figure 2B, and unsteady pressure data were acquired at 35 different Mach numbers ranging from 0.28 to 0.79. Figure 8 shows the contours plots of the power spectral densities of unsteady pressure for each case. Frequency is plotted as the non-dimensional Strouhal number consistent with Equation 2.

The contours of Figure 8A show a sharp peak (overlaid by the white curve) that begins around Mach 0.55 and remains intense throughout the Mach number range. The white curve in Figure 8A is a simple estimation of longitudinal standing wave resonance inside the cavity, $f = a_0/(2L)$ where a_0 is the stagnation speed-of-sound. The dashed, black curves indicate the cut-on frequencies of the cavity-tunnel section, $f_{CT_{cr}}$ for the first two duct modes, while dotted-dashed curves indicate the cut-on frequencies of the tunnel, $f_{T_{cr}}$. The solid black curves indicate the first three Rossiter modes (Equation 2 with m = 1, 2 and 3), the first mode being the lowest. The peaks at very low frequency ($fL/U_\infty \approx 0.1$) were likely caused by the wind-tunnel motor. The other sharp peaks in the spectra fall within the window $f_{CT_{cr}} < f < f_{T_{cr}}$, the region were trapped modes can occur[11]. A broader, weaker peak appears to agree well with the first Rossiter mode prediction, but the sharp dominant peak between Mach 0.55 and Mach 0.79 clearly agrees with the standing wave frequency estimation and appears to be the product of a trapped mode.

Figure 8B shows the power spectral density of unsteady pressure at the upstream (i.e. aft-facing) wall of the cavity when the solid Plexiglas wall is replaced by the acoustic muffler. The sharp dominant peak seen in Figure 8A is no longer evident, and over much of the Mach number range, the less intense pressure peaks show good agreement with the predicted Rossiter modes. Acoustic resonance still appears to play an important role above Mach 0.55 where the values for the second Rossiter mode (second black curve from the bottom) and the cavity standing wave (white curve) intersect and remain fairly close together. Regardless of whether some effect of the trapped mode response remains, the strong differences between Figures 8A and 8B suggests that its influence has been minimized for this wind-tunnel geometry.

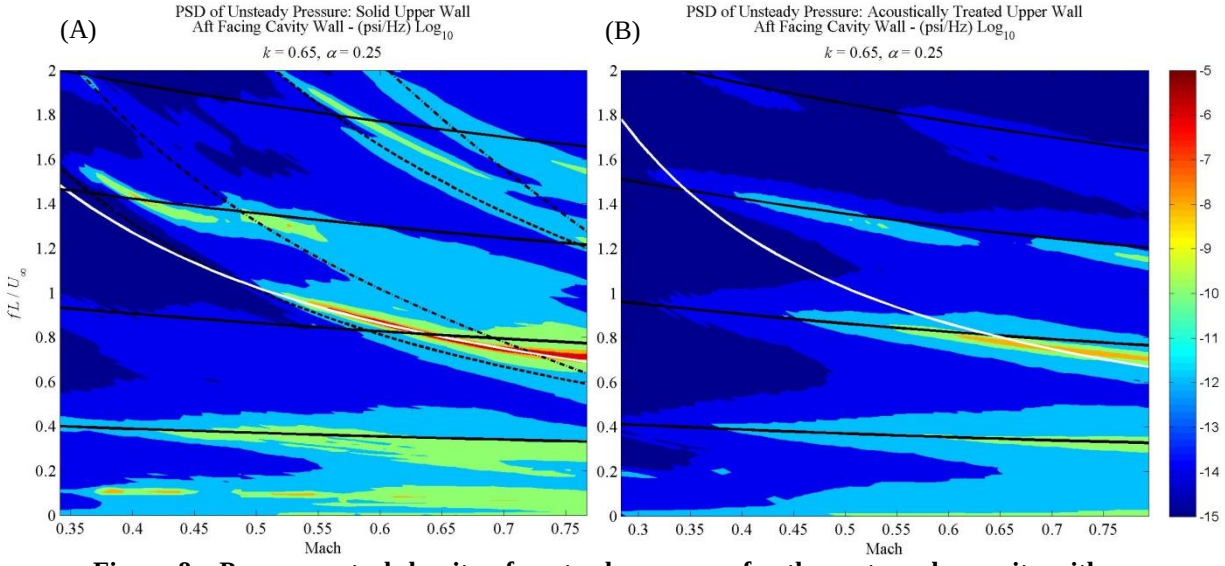

Figure 8: Power spectral density of unsteady pressure for the rectangular cavity with a solid upper wall (A) and an acoustically treated upper wall (B). The white, solid curves represent longitudinal, standing wave frequencies ($a_o/2L$). The black, solid curves are the Rossiter modes (Equation 2 with m = 1, 2, 3 and 4 from bottom to top). The black, dashed curves in (A) represent the critical cavity-tunnel cut-on frequencies, $f_{CT_{cr}}$ for the first two modes, while black, dotted-dashed curves indicate the cut-on frequencies of the tunnel, $f_{T_{cr}}$.

IV. Conclusions

The Phase 1 experiment demonstrated that a resonant cavity shear layer with a single dominant frequency was sufficiently regularized for feed-forward, adaptive-optic correction. The resonance resulted from the compatibility between the natural frequency of the cavity (longitudinal standing wave), the shear layer velocity and trapped duct modes, an effect of the cavity-tunnel geometry as described by Ref. 11. The adaptive-optic correction significantly improved the phase-averaged wavefront and its associated far-field performance. The unsteady pressure within the cavity was used to provide a reliable phase reference for the shear layer motion.

In the 180° phase case, the corrected phase-averaged wavefronts actually yielded a decreased Strehl ratio from the uncorrected case. At the time of writing, it remained unclear if this was the result of compounded errors or a single large error. The correction scheme was based entirely off of the dominant disturbance frequency (~1140 Hz) and did not account for possible effects of the first shear layer mode (~430 Hz). Perhaps more importantly, the amplitude of the DM correction and the required DM trigger delay had to be determined manually. This was accomplished by observing a Malley Probe jitter signal on an oscilloscope as the correction was applied. Adjustments were made to both phase (trigger delay) and amplitude (actuator voltages) of the correction until it appeared that the jitter signal on the oscilloscope was minimized. Although hardly elegant, this was the only feasible approach at the time. Improved adaptive-optic correction throughout the disturbance cycle almost certainly requires improved reference phase detection, wavefront measurement techniques and deformable mirror control. Nightingale *et al.*[16] have proposed a type of FFAO correction scheme which automatically adjust the DM phase and amplitude based on a reference jitter source, similar to a Malley Probe beam. Such a control scheme may be well suited to a passively forced shear layer.

The experiments of Phase 2 demonstrated that the strong resonance observed in Phase 1 resulted from the presence of trapped duct modes. The installation of an acoustically treated wall opposite the cavity appeared to nullify the trapped mode effect and restore the Rossiter mode-type oscillations. Even with the acoustically treated wall, standing wave resonances appeared to have an effect on the strength of the oscillations at higher Mach numbers. With regard to FFAO wavefront correction, however, the installation of the acoustically treated wall had the duel effect of blocking optical access and removing the dominant shear layer mode which was pivotal to the success of the FFAO correction. Follow-on attempts to passively regularize the shear layer and correct its associated aero-optic distortion will continue to involve the excitation of acoustic and hydrodynamic resonances while avoiding trapped duct modes.

Acknowledgments

The work presented in this paper was supported by the USAF AFRL/RDSA, with Drs. Larry Weaver and Frank Eaton each serving as the program manager. The views presented are those of the authors and not necessarily those of AFRL or US Government.

References

[1]Jumper, E. J., & Fitzgerald, E. J., "Recent advances in aero-optics," *Progress in Aerospace Sciences*, **37**, 299-339, 2001.

[2]Nightingale, A. M., Goodwine, B., & Jumper, E. J., "Regularizing shear layer for adaptive optics control applications," AIAA Paper 2005-4774, 2005.

[3]Duffin, D. A., Nightingale, A., & Jumper, E. J., "Feed-forward adaptive-optic correction of a regularized compressible shear layer," Ninth Annual DEPS Symposium, Albuquerque, New Mexico, 2006.

[4]Rennie, R. M., Siegenthaler, J. P., & Jumper, E. J.,"Forcing of a two-dimensional, weakly-compressible subsonic free shear layer," AIAA Paper 2006-561, 2006.

[5]Krishnamurty, K., "Acoustic radiation from two-dimensional rectangular cutouts in aerodynamic surfaces," *NACA TN 3487*,1955.

[6]Roshko, A., "Some measurements of flow in a rectangular cutout," *NACA TN 3488*, 1955.

[7]Plumblee, H. E., Gibson, J. S., & Lassiter, L. W., "A theoretical and experimental investigation of the acoustic response of cavities in an aerodynamic flow," *WADD TR-61-75*, 1962.

[8]Rossiter, J. E., "Wind-tunnel experiments on the flow over rectangular cavities at subsonic and transonic speeds," Aeronautical Research Council Reports and Memo No. 3438, 1964.

[9] Heller, H. H., Holmes, D. G., & Covert, E. E., "Flow-induced pressure oscillations in shallow cavities," AFFDL-TR-70-104, 1970.

[10]Rockwell, D., & Naudascher, E., "Review – Self Sustaining Oscillations of Flow Past Cavities," *Transactions of*

the ASME I, Journal of Fluids Engineering, **100**, 152-165, 1978.
[11]Kerschen, E. J., & Cain, A. B., "Aeroacoustic mode trapping for a wind tunnel with a cavity in the wall," AIAA Paper 2008-4213, 2008.
[12]Alvarez, J. O., & Kerschen, E. J., "Influence of wind tunnel walls on cavity acoustic resonances," AIAA Paper 2005-2804, 2005.
[13]Gordeyev, S., Jumper, E. J., Ng, T., & Cain, A. B., "Aero-optical characteristics of compressible, subsonic turbulent boundary layers," *AIAA Paper 2003-3606*, 2003.
[14]Duffin, D. A., "Feed-Forward Adaptive-Optic correction of aero-optical abberations caused by a two-dimensional heated jet," *AIAA Paper 2005-4776*, 2005.
[15]Nightingale, A. M., Goodwine, B., Lemmon, M., & Jumper, E. J., "Feedforward adaptive-optic system identification analysis for mitigating aero-optic disturbances," *AIAA Paper 2007-4013*, 2007.
[16]Nightingale, A. M., Duffin, D. A., Lemmon, M., Goodwine, B., & Jumper, E. J., "Adaptive-optic correction of a regularized compressible shear layer," *AIAA Paper 2006-3072*, 2006.